IUTAM Symposium on Computational Aero-Acoustics
for Aircraft Noise Prediction

Reprint of: CAA Broadband Noise Prediction for Aeroacoustic Design ☆

R. Ewert[a], J. Dierke[a], A. Neifeld[a], C. Appel[a], M. Siefert[a], O. Kornow[a]

[a]*Institute of Aerodynamics and Flow Technology, Technical Acoustics Branch, German Aerospace Center (DLR), Braunschweig / Germany*

Abstract

The current status of a hybrid RANS/CAA approach for the simulation of broadband sound generation is presented. The method rests on the use of steady Reynolds Averaged Navier-Stokes (RANS) simulation to prescribe the time-averaged motion of turbulent flow. By means of synthetic turbulence the steady one-point statistics (e.g. turbulent kinetic energy) and turbulent length- and time-scales of RANS are translated into fluctuations of turbulent velocity (or vorticity), whose statistics very accurately reproduce the spatial target distributions of RANS. The synthetic fluctuations are used to prescribe sound sources which drive linear acoustic perturbation equations. The whole approach represents a methodology to solve statistical noise theories with state-of-the-art Computational Aeroacoustics (CAA) tools in the time-domain. A brief overview of the synthetic turbulence model and its numerical discretization in terms of the Random Particle-Mesh (RPM) and Fast Random Particle-Mesh (FRPM) method is given. Results are presented for trailing edge, slat, jet, and combustion noise. Some problems related to the formulation of vortex sound sources are discussed.

© 2010 Published by Elsevier Ltd. Open access under CC BY-NC-ND license.
Keywords: CAA, RPM, airframe noise, slat noise, trailing edge noise, jet noise, combustion noise

1. Introduction

The development of a hybrid RANS/CAA based prediction methodology is driven by the fact that it offers the possibility to predict broadband sound at much lower computational cost compared to highly resolved unsteady CFD simulations. For the next generation of commercial transport aircraft challenging noise reduction targets are envisaged, which can only be accomplished if noise reduction technology is maximized in its performance and geometrical settings are used, which are optimized with respect to their aeroacoustic characteristics. This demands for an extensive application of CAA and brings into sharp focus the need for improved and validated CAA noise prediction methods that can be applied with confidence to new configurations within timescales which are acceptable for industry design cycles (simulations that run in hours rather than weeks). Even optimistic estimates show that highly resolved unsteady CFD simulation cannot provide computational times low enough for design purposes within the next decade. Hybrid RANS/CAA methods have the potential to fill the current simulation gap. However, in order to be applicable hybrid RANS/CAA prediction methods have to be successfully validated against experiments, especially to demonstrate their capability to properly predict design and flow changes based on just one single calibration of the model parameters.

We apply a 4D space-time model for synthetic turbulence, which was introduced in recent work. The Random Particle Mesh (RPM) method [1, 2, 3, 4] and the Fast Random Particle Mesh (FRPM) [4, 5] approach are two alternative numerical discretization of the same underlying mathematical model. Note, the underlying mathematical framework will hereafter be abbreviated as (F)RPM to distinguish it from mere numerical discretization issues. (F)RPM has a

depth that allows to reproduce a rich variety of turbulence features, such as inhomogeneous and anisotropic fields, turbulence convection at local velocities, different turbulent time de-correlation models, as well as different shapes of turbulence spectra [5]. Target values for the local length scale tensor and the turbulent stress tensor can be realized very accurately.

A first stochastic method to generate spectra and correlation functions of turbulence, which is based on random Fourier modes, was introduced by Kraichnan in the early 1970s [6]. A modified version of this approach was applied by Béchara et al. [7] to model noise sources of free turbulent flows. Further improvements of the stochastic noise generation and radiation (SNGR) method were introduced by Bailly and Lafon [8, 9] and Billson et al. [10]. In Dieste & Gabard a (F)RPM like approach was adopted to simulate trailing edge noise [11]. A wall induced turbulent upwash velocity was generated from the stochastic model to prescribe airframe noise sources [12].

The two alternative numerical approaches that we use for the discretization of the stochastic sound sources and different source formulations will be presented in Section 2. Sample results are presented and discussed for generic trailing-edge noise problems, slat noise, and jet noise in Section 3. The conclusions are drawn in Section 4.

2. Aeroacoustic Simulation Approach

2.1. Statistical noise modeling

The Computational Aeroacoustics (CAA) simulation method applied in this work provides a framework for the solution of statistical noise theories with state-of-the-art CAA techniques. The advantage of using CAA techniques is threefold. Firstly, CAA includes the effect of refraction in non-uniform flow and complex geometry. Secondly, the derivation of source statistics from RANS allows to extend the applicability of statistical noise theories to far more complex problems as being studied with analytical approaches, refer to the 3D side edge example presented herein. Thirdly, provided the simulation approach is well enough validated, a unified simulation method is accomplished, which makes feasible the broad application of statistical noise theory in an industrial environment.

Statistical noise source modeling is very closely related to the acoustic analogy concept, in which the sound generated by turbulent flow is reformulated as an acoustic wave equation forced by a source, which is a function of fluctuating turbulent quantities. Already with the introduction of the acoustic analogy concept by Lighthill [13] an expression was derived, that gives the acoustic far-field spectrum in terms of the statistics of the Lighthill tensor.

In all acoustic analogy approaches the acoustic problem is given in form of a forced linear acoustic wave equation with wave operator $\mathcal{L}$, acoustic variable p, and source q_s, which reads in the time domain,

$$\mathcal{L}p(\vec{x}, t) = q_s(\vec{x}, t). \tag{1}$$

From this forced wave equation an exact expression for the far-field spectrum related to variable p can be derived, i.e.

$$\hat{S}(\vec{x}, \omega) = \iint_{V_s} \int_{-\infty}^{\infty} \hat{G}^*(\vec{x}_1, \vec{x}, \omega)\hat{G}(\vec{x}_1 + \vec{r}, \omega)R(\vec{x}_1, \vec{r}, \tau) \exp[i\omega\tau] \; d\tau \; d\vec{x}_1 \; d\vec{r}. \tag{2}$$

Here $\hat{G}(\vec{x}_1, \vec{x}, \omega)$ denotes the exact Green's function associated to wave operator $\mathcal{L}$ in Eq. (1), expressed in the frequency domain and R represents the two-point cross-correlation of the source

$$R(\vec{x}_1, \vec{r}, \tau) = \langle q_s(\vec{x}_1, t_1) q_s(\vec{x}_1 + \vec{r}, t_1 + \tau) \rangle. \tag{3}$$

Note, this result follows for any acoustic analogy that formally can be expressed by Eq. (1). Statistical jet noise models, for example, make also use of the acoustic analogy of Lilley [14]. The previous result shows that the far-field spectrum is completely prescribed if the two-point cross-correlation of the source is known between points $\vec{x}_1$ and $\vec{x}_1 + \vec{r}$ and times t_1 and $t_1 + \tau$, i.e. Other turbulent statistics are unimportant for the prediction of acoustic far-field spectra. Statistical noise theories rest upon mathematical models derived from experimental findings to express the cross-correlation Eq. (3).

In the CAA based approach presented in this paper the problem defined by Eq. (1) is solved directly in the time-domain. The sound source on the right-hand side is modeled with a stochastic approach that provides synthetic fluctuations possessing a two-point cross-correlation of the same type as being used in statistical noise theory. Furthermore, the modeling approach allows to specify the local source variance as well as its length- and time-scales

exactly as prescribed e.g. by RANS statistics. Note, the derivation of Eq. (2) from Eq. (1) is still valid also in case of a synthetic source. Hence, the acoustic spectrum that follows from Eq. (2) for a specific statistical noise theory will be reproduced by a time-domain CAA method if (i) the propagation equations correspond to the Green's function used in the statistical noise model and (ii) if the stochastically generated source realizes the same two-point cross-correlation. In other words, the time-domain CAA approach provides an alternative way to solve the integral Eq. (2) by computing far-field pressure fluctuations and by deducing the spectrum from them.

Based on the previous discussion two main approaches can identified for statistical source modeling. That is (a) a statistical model is formulated for the full source term q_s, i.e. Eq. (3), or (b) a statistical model for a fluctuating turbulent sub-quantity, e.g. turbulent velocity, is realized based on which eventually the full source term q_s is computed thanks to the explicit source description given by acoustic analogy. The equivalent noise source model of Tam & Auriault [15] could be regarded as to belonging to the first, i.e. full source term, approach.

We will apply in this paper both approaches. For airframe noise, fluctuating velocity and vorticity are modeled, from which the acoustic source term will be derived. Jet noise is modeled with the Tam & Auriault approach.

2.1.1. Random Particle-Mesh method

The (F)RPM framework was was introduced in Refs.[1, 2, 3, 4] as a stochastic method to generate synthetic turbulence with locally prescribed one- and two-point statistics, with special focus of its applicability in CAA. It provides in an Eulerian frame a statistically stationary fluctuating sound source, which combines source convection with a temporal de-correlation mechanism. Due to the interconnection of temporal and spatial properties the method is considered a 4D synthetic turbulence model.

Two different numerically methods have been introduced in previous work for the discretization of the (F)RPM approach. Both approaches have in common that convecting particles are used, which carry random values. The concept of random particles emerges if the computational source domain is divided into N non-overlapping control volumes (CV). The boundary of each CV represents a liquid line that floats with the mean-flow field such that each CV encompasses an invariant fluid mass δm_k and the position of its center of mass (CM) $\vec{x}_k^c(t)$ is moving. For sufficient small CVs the CM drift velocity corresponds to the mean-flow velocity at the CM position [3]. A particle with associated random variables having features as speficied below is related to each CM. Then a fluctuating variable ψ_i is obtained by computing the weighted sum over all N particles evenly distributed over the resolved source region [3], i.e.

$$\psi_i(\vec{x}, t) \simeq \hat{A}(\vec{x}) \sum_{k=1}^{N} G\left(\vec{x} - \vec{x}_k^c(t)\right) \frac{r_{ik}(t)}{\rho_0(\vec{x}_k^*)}. \tag{4}$$

The quantity r_{ik} denotes the ith component of m random variables associated to each particle. The scaling $\hat{A}$ realizes a local target variance of ψ_i. Here it is assumed to be a function of $\vec{x}$, but it could be also taken at particle position $\vec{x}_k^*$. The number of components realized depend on the kind of source application. For example, for the generation of velocity fields in two spatial dimensions one scalar field is used ($m = 1$), in 3D three fields must be chosen ($m = 3$). G is a Gaussian filter kernel

$$G(\vec{x} - \vec{x}_k^c) = \exp\left(-\frac{\pi}{2} \frac{|\vec{x} - \vec{x}_k^c|^2}{l_s^2}\right), \tag{5}$$

where l_s denotes a length scale. The $m \times N$ random variables r_{ik} in Eq. (4) are defined by

$$\langle r_{ik}(t) \rangle = 0 \tag{6}$$

$$\left\langle r_{ik}(t) r_{jl}(t) \right\rangle = \delta m_k \delta_{ij} \delta_{kl} \exp\left(-\frac{|\tau|}{\tau_s}\right) \tag{7}$$

$$\tag{8}$$

In other words, the r_{ik} represent mutually un-correlated random variables with vanishing mean, a variance proportional to δm_k, showing an exponential time-correlation with time scale τ_s. The random variables are associated to the drifting particle locations $\vec{x}_k^*(t)$. To have the desired propterties, each random variable r_{ik} is generated by an Ornstein-Uhlenbeck process

$$\dot{r}_{ik} = -\frac{1}{\tau_s} r_{ik} + \sqrt{\frac{2}{\tau_s}} s_{ik}. \tag{9}$$

A (temporal) white-noise source term s_{ik} appears on the right-hand side, with properties

$$\langle s_{ik}(t) \rangle = 0 \tag{10}$$

$$\left\langle s_{ik}(t)s_{jl}(t+\tau) \right\rangle = \delta m_k \delta(\tau) \delta_{ij} \delta_{kl}. \tag{11}$$

In other words, s_{ik} represents (temporal) white-noise scaled with a factor of magnitude δm_k. The Langevin equation (9) can be solved numerically by the finite-difference equation, see e.g. Pope [16] pp. 484,

$$r_{ik}(t+\Delta t) = \left(1 - \frac{\Delta t}{\tau_s}\right) r_{ik}(t) + \left(\frac{2\delta m_k \Delta t}{\tau_s}\right)^{1/2} \sigma_{ik}(t), \tag{12}$$

where $\sigma_{ik}(t)$ are $m \times N_p$ mutually uncorrelated standardized Gaussian random variables ($\langle \sigma_{ik}(t) \rangle = 0$, $\left\langle \sigma_{ik}(t)\sigma_{jl}(t) \right\rangle = \delta_{ij}\delta_{kl}$) which are independent of themselves at different times ($\langle \sigma_{ik}(t)\sigma_{ik}(t') \rangle = 0$, for $t' \neq t$), and which are independent of $r_{ik}(t)$ at past times (e.g., $\langle \sigma_{ik}(t)r_{ik}(t') \rangle = 0$ for $t' \leq t$. Frozen turbulence is achieved in the limit $\tau_s \to \infty$, which yields a time-independent constant variance $\left\langle r_{ik}(t)r_{jl}(t) \right\rangle = \delta m_k \delta_{ij} \delta_{kl}$.

The cross-correlation of a fluctuating quantity ψ_i generated by Eq. (4) derives as

$$\mathcal{R}_{ij}(\vec{x}, \vec{r}, \tau) = \underbrace{\frac{\hat{A}(\vec{x})\hat{A}(\vec{x}+\vec{r})}{\rho_0} l_s{}^n}_{\hat{R}} \exp\left(-\frac{|\tau|}{\tau_s} - \frac{\pi |\vec{r} - \vec{u}_0\tau|^2}{4l_s^2}\right)\delta_{ij}. \tag{13}$$

Eq. (13) is in the limit $N \to \infty$ and for constant τ_s, l_s, and ρ_0 and incompressible flow $\vec{u}_0$ an exact solution for the cross-correlation. For variable length and time scales as well as compressible flow Eq. (13) is still a very good approximation to the actually achieved cross-correlations if the fields are not varying too fast on a spatial scale defined by the local turbulent length scale l_s.

In this result $\hat{R}$ indicates the variance of the fluctuations and the remaining exponential expression indicates the normalized spatiotemporal cross-correlation of the source. All components ψ_i are mutually uncorrelated. To achieve a certain source variance $\hat{R}$ the parameter $\hat{A}$ must be chosen as

$$\hat{A} = \sqrt{\frac{\rho_0 \hat{R}}{l_s^n}}. \tag{14}$$

This equation defines the scaling of amplitude $\hat{A}$ as a function of position $\vec{x}$. However, it is also applied, if the amplitude in Eq. (4) is defined as a function $\hat{A}(\vec{x}_k^\pi)$. For the latter case it can be shown that the realized variance not exactly follows the target variance $\hat{R}$, rather an effective variance is achieved, which is the target variance smoothed out with a normalized Gaussian filter based on the local length scale l_s.

2.1.2. Discretization

In the RPM discretization approach a bundle of mean-flow streamlines covers the resolved source domain. Starting from a seeding rake in an upstream position, equidistant streamlines are generated and truncated at a desired downstream position. The width and length of this source patch defines the region where stochastic sound sources are generated.

Random particles are seeded with a constant clock rate at the foremost upstream position on each streamline. The particles drift along the streamline until being finally removed downstream. The mean-flow of RANS is taken to prescribe this source convection. The spatial filtering is conducted sequentially. In the first step the random values are filtered along the streamline. Next, the values are weighted and distributed in direction normal to the streamline onto the CAA mesh. Note the streamlines usually exhibit a slight curvature such that the sequence of 1D discrete filtering steps occurs not exactly along orthogonal coordinate directions. The error is usually negligible.

In the second Fast RPM (FRPM) approach a Cartesian auxiliary mesh is used to resolve the desired source region, on which random particles are evenly distributed. Through area weighting from the surrounding corners of a hosting mesh cell the convection velocity $\vec{u}_0$ is approximated at a specific particle position. Subsequently the particle is convected further on. In a next step based on the new particle position the random values are interpolated onto the

auxiliary mesh, which is subsequently used to filter the field. Finally, the filtered values are interpolated onto the CAA mesh. More details can be found in Ref.[4].

The second approach mainly has the advantage that more easily recirculation areas in the convection velocity fields $\vec{u}_0$ can be realized, which would involve closed streamlines in the first approach. Secondly, it has the advantage to avoid the small error introduced in the RPM approach with the filtering along slightly curved lines. In the FRPM approach very efficient Gaussian filters based on recursive filters can be used [5], which allow to reduce the filtering effort more than one order of magnitude (compared to a naive application of sequentially 1D Gaussian filtering).

2.2. Sound sources

2.2.1. Vortex sound source

For the simulation of airframe noise we apply Acoustic Perturbation Equations (APE-4) with sources (for their formulation refer e.g. to [17]) as the acoustic propagation model. The homogeneous equation system is equivalent to the convective wave equation of irrotational flow. In previous studies off all appearing right-hand side terms a vortex force term on the right-hand side of the momentum equation could be identified as the most important source term. This source term reads

$$\vec{q}_m = -\underbrace{\vec{\omega}_0 \times \vec{u}'}_{I} - \underbrace{\vec{\omega}' \times \vec{u}_0}_{II} - \underbrace{(\vec{\omega}' \times \vec{u}')'}_{III} \tag{15}$$

The non-linear term III can be considered smaller than the linear terms I and II. The source term Eq. (15) is in general composed out of a rotational part defined by $\nabla \times \vec{q}_m \neq 0$, and an irrotational part defined by $\nabla \cdot \vec{q}_m \neq 0$. Whereas direct turbulent sound sources can be attributed to the irrotational part, the rotational part primarily is responsible for the generation of vorticity in the APE, which can be seen by taking the curl of the APE momentum equation. Altogether with the source term this yields

$$\frac{\partial \omega'}{\partial t} = \nabla \times \vec{q}_m \tag{16}$$

It shows that the induced vorticity on the left-hand side is entirely controlled by the rotational part of the momentum source. The approach has the advantage that the actual dynamic of the induced vorticity very closely follows the dynamics as prescribed by the source. With a propagation model based on e.g. the linearized Euler equations (LEE) this might be not necessarily the case, since partly vortex dynamics are directly resolved by the propagation equations and partly stimulated by the source. Chances are that the effectively induced vorticity dynamic not exactly follows as intended by the source term. One essential difference that appears in comparison with traditional acoustic analogy is due to the fact that the sources not only act as a acoustic source, but rather induces vorticity as well. Sound is generated as part of the acoustic simulation process due to the interaction of the source stimulated vorticity with the airframe. This is e.g. different to other statistical airframe noise approaches which rely on the availability of a surface pressure spectrum. A vorticity based source model gives a more direct connection with turbulence properties and the generated sound.

It is well known that free turbulence radiates sound following an eight power law, whereas airframe sound generation scales with a somewhat smaller, i.e., fifth power law. Hence, for small Mach numbers, the airframe noise mechanism is clearly dominating over the sound generation process of free turbulence. This means that for airframe noise simulation the rotational part of the momentum source term is even the most important contribution.

2.2.2. Source A

Based on the source term Eq. (15) different stochastic modeling strategies are possible. We will briefly discuss two possibilities. The first variant, subsequently termed 'Source A' is based on the modeling of turbulent velocity components by (F)RPM. This is accomplished by taking one (F)RPM generated scalar quantity ψ_i as a 2D stream function (i.e. $m = 1$ for Eq. (4)) from which the two velocity components derive in 2D according to

$$u_i^t = \epsilon_{ij} \frac{\partial \psi}{\partial y_j}. \tag{17}$$

In 3D, a 3 component (i.e. $m = 3$ in Eq. (4)) realization ψ_i is taken as a vector potential from which the three velocity components in 3D derive as

$$u_i^t = \epsilon_{ijk} \frac{\partial \psi_k}{\partial x_j}. \tag{18}$$

It was shown [3] that such defined velocity components give an exact realization of homogeneous isotropic turbulence (based on Gaussian spatial cross-correlations). Anisotropy could be considered in the model as well [3], however has not been considered yet. The specific source variance to be used for (F)RPM to achieve a locally realized turbulence kinetic energy that corresponds to that given by an initial RANS computation are in 2D ($n_D = 2$) [18] and 3D ($n_D = 3$)

$$\hat{R} = \frac{4}{3\pi} \frac{l_s^2 \bar{k}}{n_D - 1}. \tag{19}$$

This variance is used in Eq. (14) to determine the appropriate (F)RPM scaling. The integral length scale of the velocity fluctuations is associated to the length scale provided by RANS ($C_\mu = 0.09$, $c_l \simeq 0.5\ldots0.8$)

$$l_s = \frac{c_l}{C_\mu} \frac{\sqrt{k}}{\omega} \tag{20}$$

Now, the source formulation 'A' is a direct evaluation of the (linear) part of the source term (terms *I* and *II*) in Eq. (15) with the derived velocities. The fluctuating vorticity needed in term *II* is derived from the synthetic turbulent velocities by fourth-order numerical differentiation.

(a) Instantaneous perturbation pressure   (b) Spectra at 287° polar angle
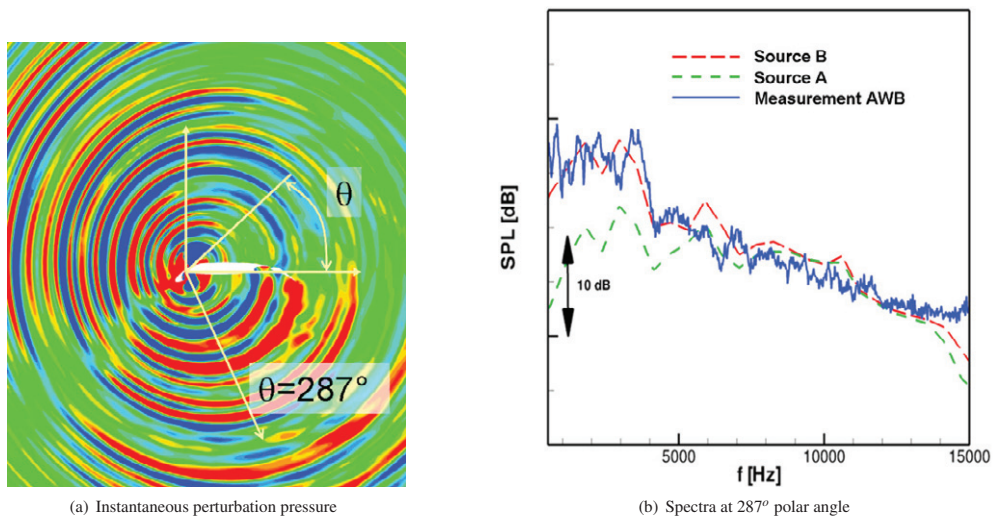
Figure 1: Slat noise simulation and measurement

2.2.3. Source term B

Alternatively, the vorticity in term II could be simulated directly by (F)RPM. In 2D a scalar quantity generated by (F)RPM could be interpreted as the 3-component of the fluctuating vorticity (ω_3'). One often made assumption is that the vorticity components are un-correlated to the velocity fluctuations, i.e. vorticity could be generated by an additional mutually un-correlated (F)RPM realization. Much easier so, for the source option 'B' we assume that the contribution of term *I* has less importance than term *II* and model only term *I*, i.e. $q_m = -\vec{\omega}' \times \vec{u}_0$. For the 2D source formulation B the variance of the fluctuating quantity provided by (F)RPM has to be matched to the 3-component vorticity variance. To achieve vorticity levels proportional to those obtained from the differentiated velocity fields used in Source A, the vorticity variance must scale according to

$$\left\langle \omega'^2 \right\rangle \propto \frac{k}{l_s^2} \propto \omega, \tag{21}$$

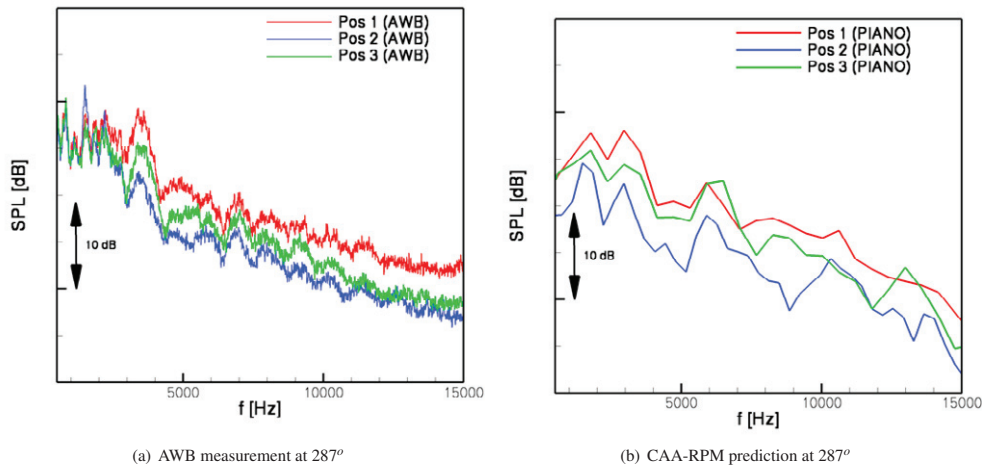(a) AWB measurement at 287°   (b) CAA-RPM prediction at 287°

Figure 2: Measured and predicted narrow-band spectra for 3 slat setting positions

where l_s and k is the length scale and the turbulence kinetic energy from RANS, respectively, and ω denotes the specific dissipation rate. The integral length scale of vorticity is also matched to length scale l_s, to comply with the behavior that can be derived for Source A. Note, in principle the integral length scale should be proportional to the Taylor length scale, which has for high Reynolds numbers an intermediate size between the Kolmogorov length scale and integral length scale l_s. However, the (F)RPM generated spectra can be deemed to represent a truncated part of the full turbulent spectrum, i.e. including the sound generated by the most energetic part of the turbulent spectrum and omitting the high-frequency contribution of smaller turbulence. Hence, the generated Gaussian spectrum should be seen as a model to describe a truncated full turbulent spectrum. Consequently, the vorticity spectrum derives only from resolved velocity components, thus exhibiting a larger length scale proportional to l_s.

The main difference between the source formulation A and B rests on the effectively used vortex model. In the source formulation A, each particle represents a vortex of form

$$\omega \propto (1 - \alpha r^2) \exp(-\alpha r^2). \tag{22}$$

This vortex model was used by Townsend (1976) [19] as an eddy function to estimate the two-point correlation tensor of fluctuating velocities in a shear flow. One specific feature of this vortex is that its first moment vanishes such that its overall circulation equals zero. As a consequence, there will be no velocity field induced outside the vortex core.

The vortex model associated to each random particle in the source model B is based on the axisymmetric Burgers (1948) vortex of form

$$\omega \propto \exp(-\alpha r^2). \tag{23}$$

This model vortex has a non-vanishing first moment and circulation, respectively, and as such the induced velocities are not restricted to the vortex core. In this case the decay of turbulent velocity occurs due to the cancellation effect of all randomly fluctuating vortices and is not modeled as part of the eddy model.

2.3. Jet Noise Sources

A primal (time-domain) formulation of the Tam & Auriault jet noise model can be achieved if a scalar (F)RPM source is directly associated with the source term Dq_s/Dt of Tam & Auriault [15] (and using a simplified convection field just depending on x-direction). This is accomplished with a scaling

$$\hat{R} = \frac{\hat{q}_s^2}{c^2 \tau_s^2} \tag{24}$$

The explicit definition of the right-hand side can be found in [15]. Using a constant convection velocity $\vec{u}_0 = (\bar{u}, 0, 0)^T$ the cross-correlations generated by (F)RPM is

$$\left\langle \frac{Dq_s(\vec{x}_1, t_1)}{Dt_1} \frac{Dq_s(\vec{x}_1 + \vec{r}, t_1 + \tau)}{Dt_2} \right\rangle = \hat{R} \times \exp\left\{ -\frac{|\tau|}{\tau_s} - \frac{\ln(2)}{l_s^2} \left[(r_1 - \bar{u}\tau)^2 + r_2^2 + r_3^2 \right] \right\}. \tag{25}$$

Two differences to the genuine cross-correlation model used by Tam & Auriault in their formulation appear here. Firstly, in the exponential function $|r_1|/\bar{u}$ is substituted for $|\tau|$. The RPM generated fluctuations satisfy approximately Taylor's convection hypothesis, which would allow to substitute $|\tau|$ for $|r_1|/\bar{u}$ in the Tam & Auriault model and thus the cross-correlations would be equal to Eq. (25). However, strictly speaking, due to the temporal decay the two-point correlations do not describe exactly frozen turbulence. Hence, the cross-correlation used in the Tam & Auriault model and Eq. (25) are not exactly equivalent. The effect this difference has on the acoustic spectrum was discussed by Morris & Boluriaan [20]. A second deviation is due to the additional dependence of the (F)RPM variance $\hat{R}$ on $\vec{r} = \vec{x}_2 - \vec{x}_1$. In the original Tam & Auriault model the variance is deemed a function of position $\vec{x}_1$ alone. Hence, for steep gradients of the source variance differences between the modeled statistical features could occur.

3. Applications

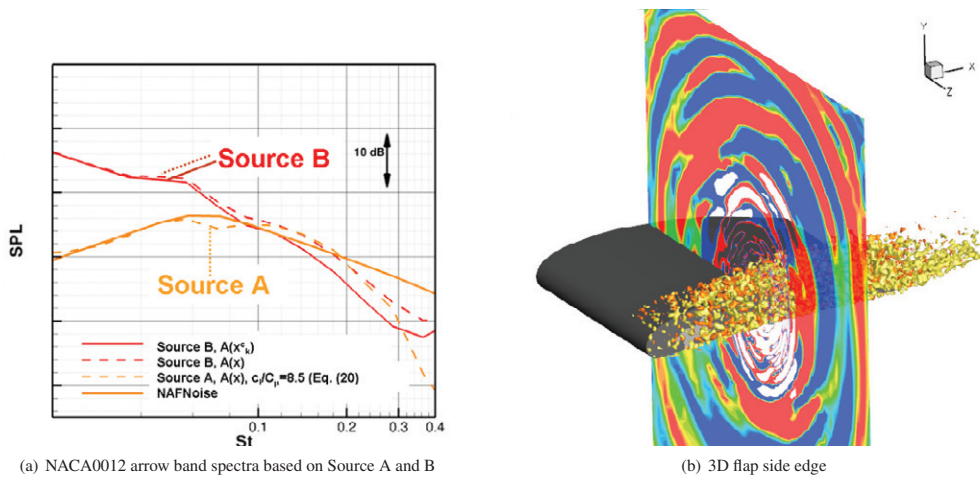(a) NACA0012 arrow band spectra based on Source A and B   (b) 3D flap side edge

Figure 3: NACA 0012 trailing edge noise spectra and 3D sources and sound field at flap side edge

3.1. Slat Noise

Results of slat noise simulations based on source formulation A and B are shown in Fig. 1. The geometry corresponds to the F16 configuration with slightly modified slat and flap deflection angles (27.8^o and 35°, respectively, vs. 30° and 30° used in the original set-up). The F16 geometry is a leading-edge normal cross-section of a 3D high-lift wing (FNG wing). The modifications in slat and flap setting were applied to minimize potential flow separation on the flap. This geometry has been used in the EC project TIMPAN. The simulation where compared with measurements conducted in the AWB wind tunnel at DLR. The hybrid RANS/CAA predictions are based on a Menter SST two-equation turbulence model for the RANS part and are performed with the DLR code TAU. The CAA simulations were performed with the DLR code PIANO.

Fig. 1 shows a comparison of simulated and measured narrow band spectra at a microphone position beneath the high-lift airfoil and perpendicular to the wind tunnel flow. The solid line refers to the measurement, the dashed lines

correspond to simulations. The simulations were based on an high-lift airfoil in free flow at 6° angle of attack (AoA). In the experiments an angle of attack of 17° was used, which gives good agreement of the measured and simulated pressure distribution around the high-lift slat and leading edge. The red dashed line in Fig. 1 is related to a simulation with Source B, i.e. a direct model for the turbulent vorticity. The prediction shows very close agreement in trend compared to the measurement. The level off-set of the simulation has been calibrated to the experimental level; no frequency shift was applied to the simulation data. Within EC project TIMPAN it was shown that based on one level calibration, it was possible to predict with considerable accuracy the acoustic level changes due to a change of gap and overlap of the slat by means of simulation. Fig. 2 gives a comparison between measurement and prediction for three settings. Details can be found in [21]. However, for Source A (green dashed line), which is based on the modeling of turbulent velocities, the low frequency part of the spectrum shows some clear deviations from the measurement and the prediction based on Source B, hence indicating that for slat noise simulations Source A is less suitable.

3.2. Trailing edge noise

For trailing edge noise of a NACA 0012 airfoil results for Source A and Source B are shown in Fig. 3(a). The CAA simulations are compared to NAFNolise/BPM predictions (solid orange line), a semi-empirical model based on NACA 0012 measurements. The test case parameters are 0° AoA, a chord length of 0.22m, and 50m/s flow speed. One-third octave spectra are plotted over Strouhal number based on the boundary layer momentum thickness. Fig. 3(a) also shows the influence of scaling the synthetic fluctuations based on an amplitude $\hat{A}$ either depending on $\vec{x}$ or on $\vec{x}''$, refer to Eq. (14) and the related discussion for a closer discussion of amplitude scaling. For Source A a good agreement is achieved between the NAFNoise/BPM prediction and the CAA simulation. The peak Strouhal number as well as the slope of the spectrum matches the prediction for Strouhal numbers smaller than 0.2. For higher Strouhal numbers a steeper drop-off is observed in the CAA simulation. The capability of Source A to properly predict changes in the flow parameters was already shown in [17] by comparing simulations with the measurements of Brooks & Hodgson [22]. A good agreement of the predicted trends was found in [17]. On the contrary, based on Source B (red curve, Fig. 3(a)) the spectrum shows mainly a constant drop-off over frequency. More precisely, the spectrum has no explicit maximum (or this is shifted to very low St-numbers), the slope is slightly too steep and the levels are over predicted in the low-frequency regime.

As a preliminary conclusion, it was found that Source B is better suited for slat noise predictions, while Source A apparently makes the better prediction for generic trailing edge noise.

3.3. Flap Side Edge Noise

First work started on the simulation of sound generation at an isolated 3D flap side edge. The intention of this work was to demonstrate in a first step the applicability of the approach for 3D airframe noise problems. First results are shown in Fig. 3(b).

3.4. Jet Noise

In some ongoing work the prediction capability of (F)RPM for jet noise is studied. The Tam & Auriault equivalent sound source model is realized with (F)RPM for a direct (primal) time-domain CAA simulation. For a single stream jet Fig. 4 presents a snapshot of a (F)RPM generated jet noise source term based on the cross-correlation model of Tam & Auriault and the radiated sound field. Fig. 4 shows a spectrum at 90° to the jet axis. The spectral shape is compared to the G-noise spectrum proposed by Tam to describe the sound radiated from fine scale jet turbulence. Good agreement is found over the entire frequency range from $St = 0.1$ to $St = 10.0$ (covering 2 orders of magnitude!).

4. Summary and conclusions

An overview was given for a hybrid RANS/CAA prediction method for broadband noise. It was argued that the approach can be deemed a simulation framework for the solution of statistical noise models with state-of-the-art CAA tools in the time domain. The simulation times are perhaps short enough to enable already today the use in industrial design. Results for different noise problems were presented. Good agreement could be found between measured and predicted spectra for trailing edge noise and slat noise. For jet noise, the general shape of the G-Noise spectrum proposed by Tam could be identified in the simulation. For the simulation of airframe noise problems, different kinds

(a) Tam & Auriault equivalent sound sources
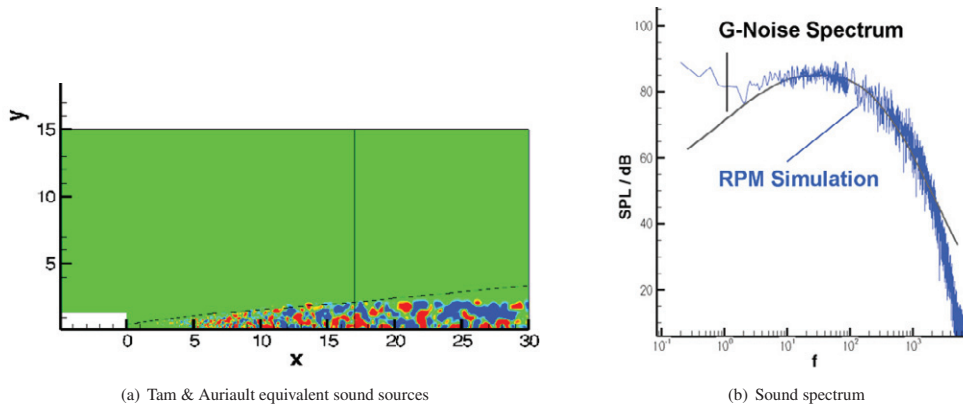

(b) Sound spectrum

Figure 4: Time domain Tam & Aurialut jet noise prediction

of noise source formulations were found to perform best for different problems. However, the best source formulation identified for each class of problems provides in its area of validity a good prediction capability of design deltas. In future work the focus will be on the formulation of a unified vortex sound source model, which can be used as well e.g. for trailing edge and slat noise problems.

[1] R. Ewert, R. Edmunds, CAA slat noise studies applying stochastic sound sources based on solenoidal digital filters, in: AIAA 2005-2862, Monterey, California, 2005.
[2] R. Ewert, Slat noise trend predictions using CAA with stochastic sources from a random particle mesh method (RPM), in: AIAA 2006-2667, Cambridge, Massachusetts, 2006.
[3] R. Ewert, Broadband slat noise prediction based on CAA and stochasic sound sources from a fast random particle-mesh (RPM) method, Computers & Fluids 37 (2008) 369–387.
[4] R. Ewert, RPM - the fast Random Particle-Mesh method to realize unsteady turbulent sound sources and velocity fields for CAA applications, in: AIAA 2007-3506, Rome, Italy, 2007.
[5] M. Siefert, R. Ewert, Sweeping sound generation in jets realized with a random particle-mesh method, AIAA Pap. 2009-3369.
[6] R. Kraichnan, Diffusion by a random velocity field, Physics of Fluids 13 (1970) 22–31.
[7] W. Bechara, C. Bailly, P. Lafon, S. Candel, Stochastic approach to noise modelling for free turbulent flows, AIAA Journal 32 (3) (1994) 455–463.
[8] C. Bailly, P. Lafon, S. Candel, Computation of noise generation and propagation for free and confined turbulent flows, in: AIAA 1996-1732, State College, Pennsylvania, 1996.
[9] C. Bailly, D. Juve, A stochastic approach to compute subsonic noise using linearized Euler's equations, in: AIAA 1999-1872, Greater Seattle, Washington, 1999.
[10] M. Billson, L.-E. Eriksson, L. Davidson, Jet noise prediction using stochastic turbulence modeling, in: AIAA 2003-3282, Hilton Head, South Carolina, 2003.
[11] M. Dieste, G. Gabal, Synthetic Turbulence Applied to Broadband Interaction Noise, in: 15th AIAA/CEAS Aeroacoustics Conference, Miami, Florida, USA, 2009, AIAA Pap. 2009-3267.
[12] M. Howe, Trailing edge noise at low mach numbers, Journal of Sound and Vibration 225(2) (1999) 211–238.
[13] M. J. Lighthill, On sound generated aerodynamically: I. General theory, Proc. R. Soc. London Ser. A 211 (1952) 564–587.
[14] A. Khavaran, J. Bridges, Modelling of fine-scale turbulence mixing noise, Journal of Sound and Vibration 279 (2005) 1131–1154.
[15] C. Tam, L. Auriault, Jet mixing noise from fine-scale turbulence, AIAA Journal 37(2) (1999) 145–153.
[16] B. P. S, Turbulent Flows, Cambridge University Press, 2000.
[17] R. Ewert, J. Dierke, C. Appel, M. Herr, RANS/CAA based prediction of NACA 0012 broadband trailing edge noise and experimental validation, in: 15th AIAA/CEAS Aeroacoustics Conference, Miami, Florida, USA, 2009, AIAA Pap. 2009-3269.
[18] R. Ewert, O. Kornow, B. Tester, C. Powles, J. Delfs, W. Rose, Spectral broadening of jet engine turbine tones, in: AIAA 2008-2940, Vancouver, Canada, 2008.
[19] A. Townsend, The Structure Of Turbulent Shear Flow, Cambridge University Press, 1976.
[20] P. Morris, S. Boluriaan, The prediction of jet noise from cfd data, AIAA Pap. 2004-2977.
[21] R. Ewert, J. Dierke, C. Appel, M. Pott-Pollenske, M. Sutcliff, CAA-RPM Prediction and Validation of Slat Setting Influence on Broadband High-Lift Noise Generation, in: 16th AIAA/CEAS Aeroacoustics Conference, Stockholm, Sweden, 2010, aIAA Pap. 2010-3833.
[22] T. Brooks, T. Hodgson, Trailing edge noise prediction from measured surface pressures, Journal of Sound and Vibration 78(1) (1981) 69–117.